Deformations, moments, and radii of ^{182,183,184,186}W from fast neutron scattering

J. P. Delaroche, G. Haouat, J. Lachkar, Y. Patin, J. Sigaud, and J. Chardine
Service de Physique Neutronique et Nucléaire, Centre d'Etudes de Bruyères-le-Châtel, B.P. n° 561, 92542 Montrouge Cedex, France
(Received 10 March 1980)

Differential cross sections for neutron scattering from the ^{182,183,184,186}W isotopes have been measured at an incident energy of 3.4 MeV. Angular distributions have been obtained for elastic scattering and inelastic scattering to the first and second excited levels of the four isotopes. Nuclear deformations have been extracted for these nuclei from a coherent analysis which combines the data presented here with low energy neutron scattering properties and total cross sections over a wide energy range. The coupled-channel and compound nucleus formalisms were used in this analysis. Volume integrals and root mean square radii of the obtained neutron optical model potential are presented and compared to the theoretical predictions of Jeukenne, Lejeune, and Mahaux. In addition, the quadrupole and hexadecapole moments of our potential are compared to the potential moments deduced from deuteron and alpha-particle scattering measurements and to experimental charge distribution moments. Finally, matter rms radii have been estimated for the four isotopes and are compared with new Hartree-Fock-Bogolyubov calculations involving Gogny's D1 effective force.

[NUCLEAR REACTIONS ^{182,183,184,186}W(n,n), (n,n'), $E_n = 3.40$ MeV; measured $\sigma(E_n, \theta)$, $\theta = 20$–$160°$. Coupled-channel and statistical model calculations. Deduced optical potential parameters, deformation parameters, potential moments, volume integrals, and rms radii. Estimated rms matter radii.]

I. INTRODUCTION

Most of the experimental information about nuclear shapes presently available has been obtained from measurements of Coulomb excitation and electron inelastic scattering. Such measurements give some information on the charge distribution in nuclei. On the other hand, there have been scattering measurements involving light charged particles (protons, deuterons, . . .) and heavy ions with incident energies well above the Coulomb barrier in order to make negligible the Coulomb interaction effects. The purpose of these measurements is to determine the mass distribution in nuclei.

Analyses of neutron interactions with nuclei may be an alternative way of nuclear shape investigation because, unlike charged particles, neutrons interact only through the nuclear field. Such studies are now possible since high energy resolution spectrometers, which yield reliable measurements[1,2] of inelastic scattering, are available in several laboratories. In their pioneering work Glasgow and Foster[3] demonstrated in an indirect way the influence of nuclear deformations on the total cross section (σ_T) for permanently deformed nuclei, and Marshak *et al.*[4] evidenced the effects of nuclear deformations on σ_T measured with oriented and nonoriented ^{165}Ho samples. In another work, Palla[5] showed for the first time that nuclear deformation effects on neutron differential cross sections calculated for ^{232}Th and ^{238}U are important. More recently a joint analysis[6,7] of the differences in total cross sections, and elastic and inelastic scattering for the ^{148,150,152,154}Sm isotopes confirmed these effects and illustrated nicely for these nuclei the evolution from a spherical shape (^{148}Sm) to a permanent deformed shape (^{154}Sm).

The present work is devoted to the investigation of the nuclear structure of the ^{182,183,184,186}W isotopes. It is part of a systematic study performed at Bruyères-le-Châtel on nuclei in and near the rare-earth region. The W isotopes are at the rotational edge of the $A = 190$–200 transitional region, where even and odd nuclei have shapes changing gradually from prolate at the low-A end to oblate at the high-A end. In addition, it has been shown from phenomenological approaches[8,9] and Hartree-Fock-Bogolyubov (HFB) calculations[10] that the hexadecapole deformation parameters β_4 of the even W isotopes have large negative values. The level schemes (ground state and next $K \neq 0$ bands) of the tungsten isotopes are shown in Fig. 1 to illustrate the deformed character of these nuclei. We have performed elastic and inelastic scattering measurements at an incident neutron energy of 3.4 MeV. The choice for this energy relies upon Lagrange's calculations[11] which evidenced that around this kinetic energy there is a large sensitivity of the ^{182}W total cross section to variations of the quadrupole deformation parameter β_2. The experimental apparatus used for the measurements, and the data reduction are described in Sec. II. In Sec. III we present the analysis of the measurements and the method

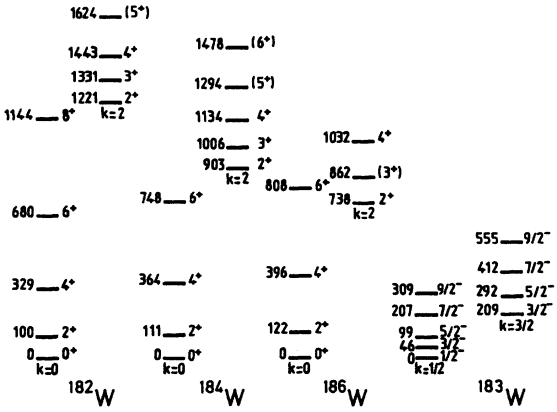

FIG. 1. Simplified level schemes of tungsten isotopes at low excitation energies. Ground states bands ($K=0$) and γ-vibrational bands ($K=2$) for the even-A isotopes. $K=\frac{1}{2}$ and $K=\frac{3}{2}$ bands for ^{183}W.

used to determine the parameters of the deformed optical potential (DOP). The results of our coupled-channel and statistical model calculations are given and discussed in Sec. IV. The DOP is then adapted for proton scattering in order to check our deformation parameters at 16 MeV incident energy for which elastic and inelastic scattering angular distributions have been measured[12] for the even W isotopes. Our study is completed by determining volume integrals and root mean square (rms) radii of the real and imaginary parts of the potential, quadrupole and hexadecapole potential moments, and rms matter radii. These average parameters are presented and discussed in Sec. V and they are compared with some corresponding deuteron and alpha particle experimental results and with theoretical predictions of the Jeukenne, Lejeune, and Mahaux (JLM) model[13,14] and HFB calculations.[10]

II. EXPERIMENTAL METHODS AND RESULTS

The differential cross section measurements were performed using the four detector neutron time-of-flight facility of the Centre d'Etudes de Bruyères-le-Châtel tandem accelerator laboratory.[15]

The incident 3.40 MeV neutrons were produced by the ^{7}Li$(p, n_0)^{7}$Be reaction using a thin target. The EN tandem Van de Graaff accelerator provided a proton beam of 5.07 MeV, pulsed at a repetition rate of 2.5 MHz and bunched into bursts with a time dispersion of 1 ns full width at half maximum (FWHM). By using a post-pulsing system, burst widths as short as 0.7 ns were achieved, as checked by time-of-flight measurement of the prompt γ rays from proton induced reactions in the target. The average current was typically 2 μA. The target consisted of 99.8% enriched ^{7}Li evaporated on a 2-cm-diam, 1-mm-thick tantalum disc. The energy spread of the incident neutrons, due to the thickness of the target, was about 25 keV for the even-A W measurements and around 10 keV for the ^{183}W ones. The energy difference between neutrons from the ^{7}Li$(p, n)^{7}$Be reaction which leave ^{7}Be in its ground state and in its first excited state (431 keV) was large enough to enable scattering measurements for the ground state and the two first excited states of each nucleus (see Fig. 1).

The primary neutrons bombarded cylindrical samples located at 0° with respect to the proton beam axis and at 10.3 cm from the target. The separated isotope tungsten samples, on loan from the USSR (Technabexport), were in the form of metallic powders. Each of them was placed in a polyethylene container 2 cm diam × 5 cm high. The four samples had the same number of atoms (0.215 mole). The dimensions, masses, and enrichments are presented in Table I.

The scattered neutrons were detected by an array of four recoil proton detectors placed at 20° intervals. Each detector consisted of a 10 cm diam × 2.5 cm thick NE-213 liquid scintillator optically coupled to an XP-1040 photomultiplier tube. Each detector was housed in a massive shield of paraffin loaded with lithium carbonate and borax. Four 1-m-long shadow bars made of polyethylene and lead intercepted neutrons from the source in the detector direction. In order to avoid illumina-

TABLE I. Characteristics of the tungsten samples.

Main isotope (At.wt)	Isotopic composition (%)					Sample		
A	180	182	183	184	186	Height (cm)	Diameter (cm)	Mass (g)
182	<0.05	91.4 ± 0.2	5.48	2.28	0.84	3.6	1.5	39.05
183	<0.03	5.12	75.0 ± 0.4	17.76	2.12	2.9	1.5	39.26
184	<0.03	0.85	1.39	94.9 ± 0.1	2.86	3.6	1.5	39.48
186	≪0.01	0.04	0.04	0.13	99.79 ± 0.03	3.4	1.5	39.91

tion of the bar tips a separate lead block was placed near the neutron source; the size and dimensions of this block depended on the location of the four-detector array. Intermediate 1.5- and 0.5-m-long collimators of paraffin loaded with lithium carbonate and borax were placed between the detector shielding and the shadow bars; they greatly reduced time-independent background in the scattered neutron spectra. The flight path from the sample to each detector was 8 m for the even-A W measurements and 10 m for the ^{183}W measurements, and the total energy resolution of the spectrometer was ≤ 50 and ≤ 28 keV, respectively. A time-of-flight spectrum for the ^{186}W sample is shown in Fig. 2 to illustrate the experimental resolution and the good separation of the scattered neutron peaks.

Data were collected using a standard electronic setup. Pulse shape discrimination was employed to reject most of the γ rays detected in the scintillators. A two-parameter data acquisition system recorded the time-of-flight and the recoil proton pulse height for each detected event. The detector pulse-height threshold has been adjusted in off-line data analysis to minimize the statistical uncertainties in the yields extracted from the time-of-flight spectra.

The primary neutron flux was monitored by using an auxiliary neutron detector in the time-of-flight mode, and also by counting with a Ge(Li) diode the 431- and 478-keV γ rays produced by proton induced reactions in ^{7}Li. The γ ray and neutron monitor indications were consistent with each other within 1% throughout the course of the measurements. The energy dependence of the detector efficiency was determined by comparing measurements of the neutron yields from the ^{7}Li$(p,n)^{7}$Be reaction for the ground and first excited states of ^{7}Be, with the known cross sections

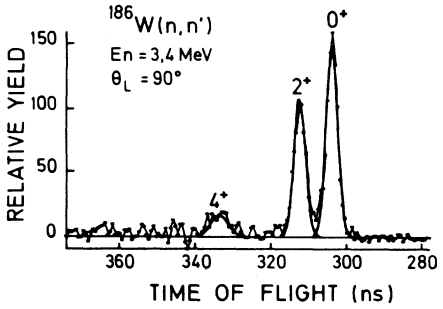

FIG. 2. Time-of-flight spectrum of 3.40 MeV neutrons scattered at 90° by ^{186}W. The flight path is 8 m. The spectrometer time resolution is $\simeq 2.3$ ns corresponding to an energy resolution of $\simeq 50$ keV. Heavy lines on this figure are standard line shapes fitted to the peaks.

for that reaction.[16] The absolute efficiency was not needed since we removed the sample and brought the detector to 0° with respect to the proton beam axis in order to measure the incident neutron flux. Hence, the incident and scattered neutron fluxes were measured with the same detector.

Measurements were made at 19 angles for each sample over the angular range 20° to 160°. In addition, runs with empty containers were taken in order to substract the polyethylene contribution to the scattering spectra. After background subtraction was achieved for each scattered neutron spectrum, yields were obtained for isolated peaks both by direct summation of counts and also by fitting standard line shapes to the peaks. For peaks too close to each other, yields were extracted by line-shape fitting procedures only. The net yields were corrected for the anisotropy of the incident neutron beam and the finite size of the sample. These latter corrections included those for neutron flux attenuation by the sample, multiple scattering, and geometrical effects; the corrections were made using the analytical method described by Kinney.[17] Since the incident and scattered neutron fluxes were measured with the same detector, normalization uncertainties were small. Uncertainties in the measurements arose from counting statistics and background subtraction, monitor counting dispersion, detector efficiency, and sample corrections. These contributions, listed in Table II, were added quadratically to give the experimental uncertainties.

The elastic scattering cross sections, measured at $E_n = 3.40$ MeV neutron incident energy, for the even-A isotopes ^{182,184,186}W are plotted in Fig. 3; the curves are the results of theoretical calculations to be described below. The essential features are directly evident from the data. One notes that for these deformed nuclei the elastic scattering angular distributions are almost identical for the three isotopes, with barely discernible differences at angles beyond the forward peak. That these nuclei have very similar scattering properties is also reflected in the inelastic scattering cross sections to the first excited 2^+ state (Fig. 4) and 4^+ state (Fig. 5). However, the slight differences in the angle-integrated inelastic scat-

TABLE II. Uncertainty estimates for cross section measurements.

Counting statistics in the peak and background subtraction	2–35%
Dispersion of monitor indications	<1%
Detector efficiency	2–4%
Sample corrections	1–3%

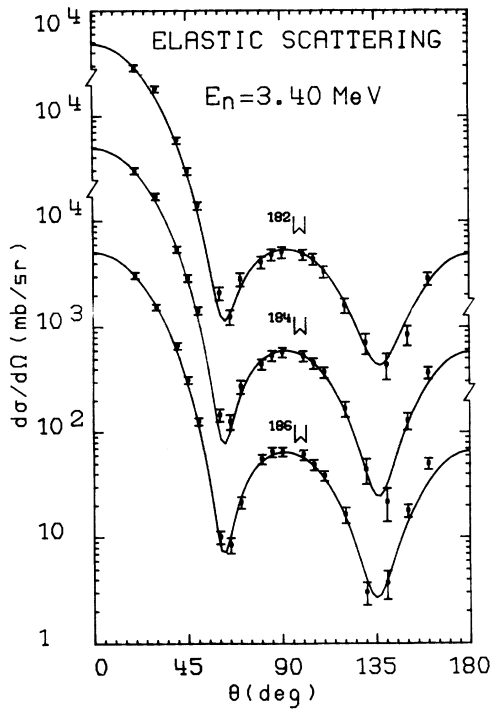

FIG. 3. Comparison at 3.40 MeV incident neutron energy of measured and calculated elastic scattering angular distributions for ^{182,184,186}W. Compound elastic scattering components are included in the calculations.

tering cross sections seem to result from the changing deformation from one isotope to the other. For the odd nucleus ^{183}W the data for elastic scattering ($\frac{1}{2}^-$) and inelastic scattering to the first $\frac{3}{2}^-$ and $\frac{5}{2}^-$ excited states are presented in Fig. 6.

III. DATA ANALYSIS

The interaction mechanism of 3.4-MeV neutrons with the W isotopes involves both direct interaction (DI) and compound nucleus (CN) processes, the mixture of which will be discussed below. To which extent the tungsten isotopes may be assumed to be rotational nuclei is reflected in Fig. 1 which shows the low energy part of the level schemes for ^{182,183,184,186}W. The sequences of low-lying energy levels[18] in the even isotopes exhibit two rotational bands built respectively on the ground state ($I^\pi = 0^+, K = 0$) and the second 2^+ excited state ($I^\pi = 2^+, K = 2$). One may notice that the level spacing in the ground state band increases with A. This trend indicates a regular decrease of the moments of inertia and the related nuclear deformations from $A = 182$ to $A = 186$. The $K = 0$ and $K = 2$ bands, moderately well separated for ^{182}W, become mixed for ^{186}W. These last properties which are the signature of nonaxial components in the deformations were carefully studied by Kumar and Baranger.[19] Kerman,[20] Rowe,[21] and Brockmeier *et al.*[22] have analyzed in detail the low-lying level properties of ^{183}W. From these works, it seems clear that Coriolis forces mix the $K = \frac{1}{2}$ and $K = \frac{3}{2}$ bands in ^{183}W. As the band mixing generally increases with the energy of the excited states, a test might be performed by comparing coupled-channel calculations involving K-mixed wave functions to measured cross sections for inelastically scattered neutrons from high-lying excited states. In the absence of such desirable data this comparison is not possible. Consequently, the only way in which our measurements can be analyzed is to assume for the tungsten isotopes a symmetric rotational model. This model is crude but offers the advantage of making easier the entire analysis of the neutron scattering data studied in the present work. Thus, the W isotopes are assumed similar in nature, the remaining differences being to a first approximation the deformation parameters which vary for the even isotopes in the way suggested by Götz *et al.*[8] and Möller *et al.*[9]

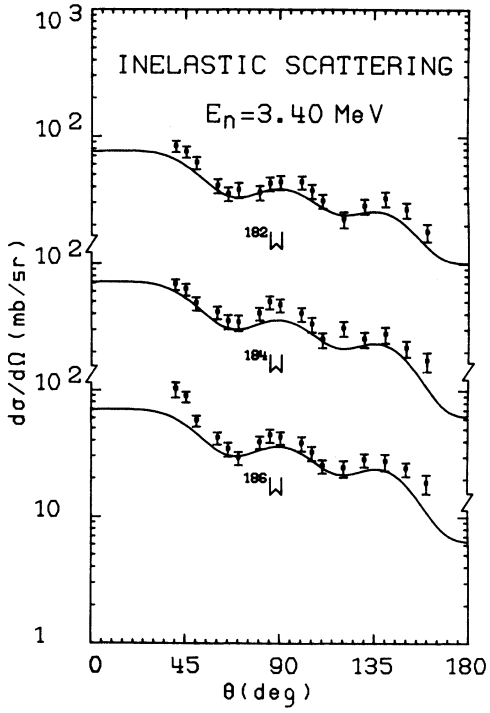

FIG. 4. Differential cross sections for 3.40 MeV neutrons scattered from the 2^+ excited states of the even W. The curves are calculations including both direct interaction and compound nucleus contributions as described in the text.

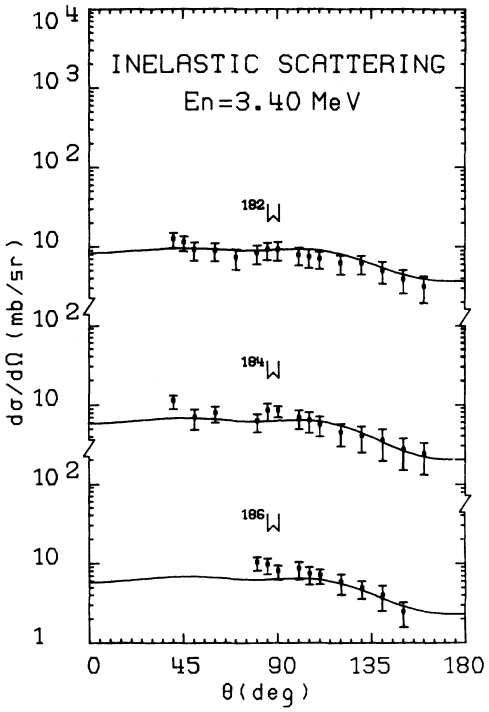

FIG. 5. Differential cross sections for 3.40 MeV neutrons scattered from the 4^+ excited states of the even W. The curves are calculations including both direct interaction and compound nucleus contributions as described in the text.

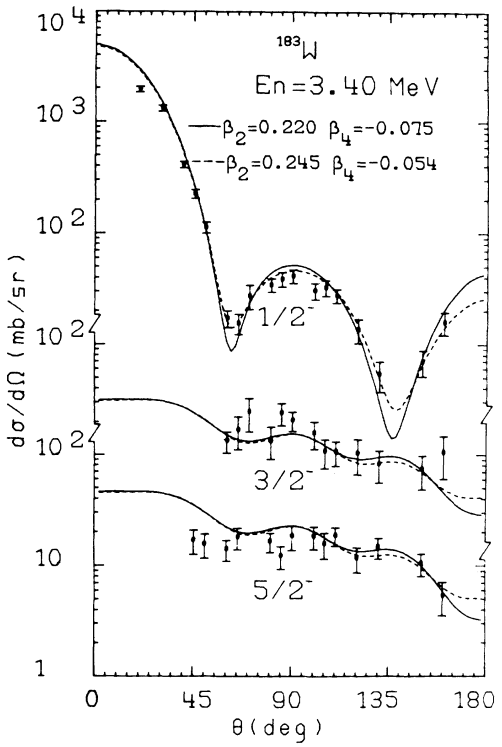

FIG. 6. Neutron elastic and inelastic scattering angular distributions at 3.40 MeV incident energy for ^{183}W. The full lines correspond to the following values of deformation parameters: $\beta_2 = 0.220$, $\beta_4 = -0.075$. The dashed lines are for $\beta_2 = 0.245$, $\beta_4 = -0.054$.

A. Methods of analysis

For our analysis we follow the method described in Refs. 7 and 23. However, the set of data involved presently is less extensive and includes some measurements whose accuracy may be questionable as discussed below. The lack of recent data especially in the low energy region (i.e., E_n < 300 keV) does increase the uncertainties on the model parameters due to the method of analysis. In the coupled-channel calculations, a unique, complex, and deformed potential was used. In addition to the systematic variations (i.e., A dependence of potential radii), the potential has been varied from one isotope to the other through the deformation parameters β_2 and β_4 and the asymmetry term $\epsilon = (N - Z)/A$. The isotopic dependent term has been assumed to be complex. The neutron data included in the analysis were (i) potential scattering radii R' (Ref. 24) and s- and p-wave strength functions S_0 and S_1 (Refs. 24–27) determined at very low incident energy, (ii) total cross sections σ_T measured by Whalen *et al.*,[28] Martin,[29] and Glasgow *et al.*,[3] and (iii) the present differential scattering cross sections at 3.40 MeV. This so-called SPRT method[23] (S and P for s- and p-wave strength functions, R for potential scattering radius, and T for total cross section) was employed to obtain a reliable set of optical potential parameters within a large energy range. The parameters were constrained to fit S_0, S_1, R', and the energy variation of σ_T with particular attention to the energy range below 1 MeV. The parameters were then slightly varied in order to optimize the fits to the differential scattering cross sections of the present work. As noted above, the compound nucleus (CN) effects are not negligible at 3.40 MeV incident energy; they were taken into account in the fitting procedure of differential scattering cross sections. The estimate of the CN cross sections was obtained from statistical model calculations by using transmission coefficients deduced from the coupled-channel calculations performed at the almost final stage of analysis. The differential scattering cross section calculations were then completed when a good fit to the data was obtained. The final results are shown in Figs. 3, 4, and 5.

B. Optical and statistical model calculations

At incident energies (E_n) below 10 MeV, where the volume absorption effects on cross sections

are generally believed[30] to be negligible, the neutron potential has the following form:

$$U = -Vf(r, a_v, R_v) + 4ia_D W_D \frac{d}{dr} f(r, a_D, r_D) + 2\lambda_\pi^2 V_{so} \vec{l}\cdot\vec{s} \frac{1}{r}\frac{d}{dr} f(r, a_{so}, R_{so}) . \quad (1)$$

The form factor f is of a Woods–Saxon type: $f(r, a_t, R_t) = \{1 + \exp[(r - R_t)/a_t]\}^{-1}$; $R_t = r_t A^{1/3}[1 + \sum_{\lambda=2,4} \beta_\lambda Y_\lambda^0(\Omega')]$ is the "nuclear" radius and (Ω') refers to the intrinsic angular coordinate system. The spin-orbit potential V_{so} has not been deformed since the effects[31] of its deformation on the calculated differential cross sections were found to be negligible. The depths of the real and imaginary surface potentials were, respectively, $V = V_0 - \alpha E - V_1[(N - Z)/A]$ and $W_D = W_0 + \gamma\sqrt{E} - W_1[(N - Z)/A]$. The symbol E represents the incident neutron energy (MeV) and α and γ the energy-variation parameters of the potential strengths. The coupling basis $(0^+, 2^+, 4^+)$ was used for the even isotopes. The equivalent basis adoped for ^{183}W was $(\frac{1}{2}^-, \frac{3}{2}^-, \frac{5}{2}^-, \frac{7}{2}^-, \frac{9}{2}^-)$. In the intrinsic coordinate system, the deformed potential (1) was expanded in spherical harmonics:

$$U(r, \Omega') = \sum_\Lambda U_\Lambda(r) Y_\Lambda^0(\Omega'), \quad \Lambda = 0, 2, \ldots \quad (2)$$

with $\Lambda \leq 8$ and complex coupling form factors. Raynal's code ECIS[32] was used to test the effects (see above) of a full Thomas-Fermi spin-orbit potential[33] on the cross sections and to perform the time consuming calculations for ^{183}W. A modified form[34] of Tamura's code[35] JUPITOR-1 was used for the other calculations. The statistical model (SM) calculations were performed by using Lagrange's *et al.* code[36] HELMAG This computer code was modified in order to include the modern[37,38] SM theories. Lagrange tested[39] their influence on neutron elastic and inelastic scattering cross sections below 2.4 MeV for some Mo isotopes and showed that the fits were improved. For the 3.4 MeV SM calculations, the predictions of Dresner's formalism[40] were compared with those of the new[37,38] ones. The differences thus obtained were negligible for the inelastic scattering cross sections. The main effect of the new theories is to reduce the compound elastic scattering cross sections by an amount of ~10%, leading to an improvement of the fits. The possibility for interference between direct and compound mechanisms was ignored. This is due to the fact that many channels are open at 3.4 MeV incident energy then making this effect negligible.[38]

IV. DISCUSSION

A. ^{182,184,186}W + n scattering

For the potential parameter search the starting values of the deformation parameters (β_2, β_4) were those from Möller *et al.*[9] These parameters and the geometrical parameters were then varied following the method explained in Sec. III. We met some unexpected difficulties while making the parameter search; that is, it was not possible to reproduce reasonably well (i.e., within a 5% accuracy) the total cross sections measured[28,29] at incident energies below 2 MeV. Our purpose in the present work is not to discuss in detail the origin of these disagreements. Thus, we adapted our method of analysis (Sec. III) by forcing the optical potential to fit the low-energy neutron scattering properties (S_0, S_1, R'), the total cross sections measured[3] at incident energy $E_n \geq 2.3$ MeV, and our elastic and inelastic scattering angular distributions corrected for estimated compound nucleus components. Furthermore, the total cross section for the element built from the calculated σ_T for the isotopes ^{182,184,186}W had to follow closely the energy variation of the measured σ_T for ^{nat}W in full energy range.[3,28,29]

The values of potential depths and geometrical parameters are given in Table III and the deformation parameters in Table IV; the potential parametrization contains energy dependences and geometries which are commonly accepted.[41] In particular, our W_D energy variation (see Table III) is found to be identical to the one given by Lister *et al.*[42] in a previous analysis of neutron differential cross sections for the even W isotopes below 1.5 MeV incident energy. A comparison between calculated and measured S_0, S_1, and R' is presented in Table V. The agreement between data and calculations is good for S_0 and R' and moderate

TABLE III. Tungsten isotopes. Neutron optical potential parameters. Strengths in MeV; geometry parameters in femtometers. Incident neutron energy E_n in MeV; $E_n < 9$ MeV.

$V = 49.90 - 16.00\left(\frac{N-Z}{A}\right) - 0.25E_n$	$W_D = 4.93 - 8.00\left(\frac{N-Z}{A}\right) + 1.30E_n^{1/2}$	$V_{so} = 6.00$
$r_V = 1.26$	$r_D = 1.28$	$r_{so} = 1.26$
$a_V = 0.63$	$a_D = 0.47$	$a_{so} = 0.63$

TABLE IV. Deformation parameters determined from the present analyses.

Nucleus	β_2	β_4
^{182}W	0.223	−0.054
^{183}W	0.220	−0.075
^{184}W	0.209	−0.056
^{186}W	0.203	−0.057

for S_1. This last result is not too surprising since the "experimental" values quoted for S_1 were not deduced from direct measurements but were derived either from capture measurements or from estimations. Thus uncertainties on these values are probably rather large. However, if one refers to Musgrove's compilation[43] devoted to S_0 and S_1, the neighboring nuclei have p-wave strength functions whose magnitude is compatible with that calculated in the present work.

A full comparison between calculated and measured total cross sections is not presented in this work but will be reported soon.[44] In short, some strong disagreements appear between the calculations and the data of Whalen *et al.*[28] and Martin.[29] However, since our optical model (OM) analysis was completed, new σ_T measurements have been performed by Whalen[45] in the energy interval 300 keV–5 MeV on the even W isotopes. The comparison between these new data and the present optical potential calculations shows that most of the discrepancies previously observed vanish. If one excepts the case of the ^{182}W total cross section below 500 keV, a satisfactory agreement is now obtained between calculations and new measurements. The discrepancies at low energy seem to be related to self-screening effects which were not taken into account.

Further and more precise tests of our analysis are shown in Figs. 3, 4, and 5 where the elastic and inelastic scattering cross sections measured at 3.4 MeV incident energy for ^{182,184,186}W are presented. The compound nucleus components are included in the curves and represent approximately 1%, 15%, and 50% of the full cross sections for the 0^+, 2^+, and 4^+ scattering cross sections, respectively. These estimates are more important than generally believed at this incident energy for such medium-mass nuclei. The fits displayed in Figs. 3, 4, and 5 are good, with comparable quality for each isotope. The analysis of these neutron scattering data shows that the deformation parameters β_2 and β_4 can be determined with good accuracy. In particular, the effect of changing the sign of β_4 is illustrated in Fig. 7 for ^{182}W; the full ($\beta_4 < 0$) and dashed ($\beta_4 > 0$) curves represent the calculated cross sections including both DI and CN contributions. The effects of variations of β_4 values, especially for the direct inelastic scattering cross sections, is large enough to be significant. Similar conclusions can be drawn for ^{184}W and ^{186}W. Calculated total cross sections at incident energies below 500 keV give results which confirm these conclusions. It is thus well established that the sign of β_4 deformations of the even W isotopes can be deduced from neutron scattering data without any ambiguity.

B. ^{183}W + n scattering

A careful comparison between cross sections for the even and odd (^{183}W) neighboring W isotopes may lead to appreciate, in addition to possible even-odd effects, the extent at which the simple rotational model could well represent the wave

TABLE V. Comparison between experimental and calculated values of the low energy neutron scattering parameters S_0, S_1, and R'.

	^{182}W		^{184}W		^{186}W	
Parameter	Exp	Calc	Exp	Calc	Exp	Calc
$S_0(\times 10^4)$	2.50 ± 0.30 [a]	2.39	2.60 ± 0.30 [a]	2.60	2.20 ± 0.30 [a]	2.72
	2.60 ± 0.54 [b]		3.00 ± 0.60 [b]		2.15 ± 0.46 [b]	
	2.40 ± 0.31 [c]		2.35 ± 0.24 [c]		2.23 ± 0.27 [c]	
$S_1(\times 10^4)$	0.30 ± 0.10 [a]	0.98	0.30 ± 0.10 [a]	0.86	0.30 ± 0.10 [a]	0.81
	$0.28 + 0.52$ [b]		$0.28 + 0.52$ [b]		$0.28 + 0.52$ [b]	
	-0.15		-0.15		-0.15	
			2.00 ± 0.50 [d]		0.76 ± 0.30 [d]	
R' (fm)	7.30 ± 0.30 [a]	7.43	7.30 ± 0.30 [a]	7.54	7.30 ± 0.30 [a]	7.64

[a] See Ref. 24.
[b] See Ref. 25.
[c] See Ref. 26.
[d] See Ref. 27.

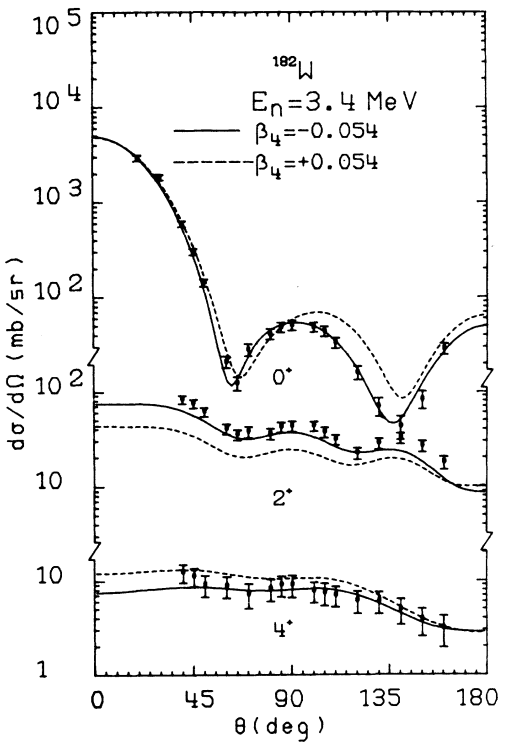

FIG. 7. Neutron elastic and inelastic scattering angular distributions at 3.40 MeV incident energy for ^{182}W showing the effects of hexadecapole deformation change (i.e., $\beta_4 > 0$ and $\beta_4 < 0$) on calculated angular distributions.

functions of low-lying excited states in the ^{183}W ground state rotational band ($I^\pi = \frac{1}{2}^-$). However, one has to notice that neutron data other than the scattering cross sections measured and presented in this paper are rather scarce. This means that uncertainties related to our method of analysis are necessarily larger for ^{183}W than for ^{182,184,186}W. Since our differential cross sections (see Fig. 6) were the unique set of data analyzed, we attempted to fit them by assuming (i) the asymmetry-dependent potential (see Table III), (ii) the multipole expansion (2) for the deformed potential, and (iii) a coupling basis ($\frac{1}{2}^-, \frac{3}{2}^-, \frac{5}{2}^-, \frac{7}{2}^-, \frac{9}{2}^-$) which may be considered as equivalent to the basis ($0^+, 2^+, 4^+$) involved in the even-W calculations. The criterion (iii) was chosen so as to make the target angular momentum transfer $\Delta I \leq 4$, related to possible transitions between collective states, common to the even and odd W isotopes. A first adjustment of the quadrupole deformation parameter β_2 for ^{183}W yielded a value $\simeq$10% higher than β_2 for ^{182}W (see Table IV). The corresponding theoretical cross sections (including CN components) are shown as dashed lines in Fig. 6. But before going further in the search of potential deformations for ^{183}W we would like to compare this preliminary value of β_2 for ^{183}W to the results of Coulomb excitation measurements,[46] studies of fragmentation of Nilsson single quasiparticle strengths and $i_{13/2}$ orbits,[47,48] and Hartree-Fock-Bogolyubov (HFB) studies.[10] The Coulomb excitation measurements[46] indicate a smooth decrease of the charge quadrupole moment with increasing mass from $A = 182$ to $A = 186$ reflecting a corresponding decrease in charge quadrupole deformations. As far as charge and potential deformations compare and reflect nuclear shapes, the present deformations β_2 for even tungsten nuclei display a variation with mass number comparable to the variation of the charge deformations. On the other hand, the preliminary value of β_2 (^{183}W) disagrees with these results. An additional argument against $\beta_2(^{183}\text{W}) > \beta_2(^{182}\text{W})$ is provided by HFB calculations[10] which indicate that the W isotopes are rigid against quadrupole deformations. As a consequence, the ground state properties (i. e., quadrupole mass deformations) must vary smoothly when one neutron or more is added to ^{182}W. Since then, Casten *et al.*[47] and Casten[48] have proposed that large hexadecapole deformation might be important for understanding the fragmentation of Nilsson model strengths and the (τ, α) and (d, t) cross sections to $\frac{13}{2}^+$ states in odd-mass tungsten isotopes. Consequently we made a new analysis of our angular distributions. Taking into account the previous information, we assumed for $\beta_2(^{183}\text{W})$ a value intermediate between $\beta_2(^{182}\text{W})$ and $\beta_2(^{184}\text{W})$, and the hexadecapole deformation parameter $\beta_4(^{183}\text{W})$ was varied in order to optimize the fits.

The adopted values for the deformation parameters β_2 and β_4 are

$$\beta_2(^{183}\text{W}) = 0.220; \quad \beta_4(^{183}\text{W}) = -0.075 .$$

If one considers that β_2 and β_4 cannot be determined separately, the above values have uncertainties probably higher than those estimated for the even-W isotopes (see Sec. V). Then the comparison between ^{183}W and ^{182,184,186}W deformation parameters indicates that β_2 decreases with increasing mass and $\beta_4(^{183}\text{W})$ is higher than $\beta_4(^{182}\text{W})$ by 40%. The value of $\beta_4(^{183}\text{W})$ that we obtained is large but consistent with $\beta_4 \simeq -0.09$ given by Casten[48] and with deformations obtained for ^{181}W by Bernthal *et al.*[49] In Fig. 6 the comparison between the new calculations (full lines) and the measured differential cross sections is shown. The CN components though small (i. e., <1 mb/sr) at 3.40 MeV, a result which is not too surprising for an odd target nucleus, were not neglected. The fits presented in Fig. 6 are satisfactory but not as good as the ones obtained for the even isotopes at the same incident energy.

In order to improve the agreement between calculations and measurements the parameters β_2, β_4, and W_D (absorptive potential) were varied. The imaginary potential might change since in addition to the asymmetry $[(N-Z)/A]$ it may depend[50] on the density of CN states leading to a possible even-odd effect. As we failed to improve the fits by slightly changing β_2, β_4, and W_D, it seems questionable to assume the simple version of the rotational model for ^{183}W if the same quality of fits to angular distributions is desired for all the tungsten isotopes. For this purpose it might be desirable to use more realistic collective wave functions in which a strong band-mixing should not be ignored.[20-22]

C. Comparison between neutron and proton scattering

Our rather extensive analysis of neutron cross sections for the tungsten isotopes has clearly shown that the deformed optical potential is asymmetry dependent. In order to test the $[(N-Z)/A]$ dependence of our potential, we analyzed proton angular distributions measured[12] at 16 MeV for the even isotopes by changing the sign of the $[(N-Z)/A]$ dependent terms in the optical potential. In other words, we were interested in knowing if it were possible to determine a consistent complex isospin potential[51] in the tungsten mass region starting from the analysis of neutron cross sections. Moreover, we took the opportunity of testing, for proton interactions, the deformation parameters (see Table IV) extracted from our neutron interaction studies.

At 16 MeV incident energy, the volume absorption W_v cannot be neglected. Following Becchetti and Greenlees,[30] W_v was assumed to be isospin independent. The energy variation of W_v was chosen to fit the data. The geometrical parameters (i.e., diffuseness and radius) were taken identical to those of the real central potential (see Table III). Furthermore, the potential W_v was deformed. We took into account the competition between surface and volume absorptions. The Coulomb radius was $R_c = 1.10\,A^{1/3}$ (fm) and the Coulomb potential V_c was deformed assuming a sharp-edge charge density form factor. We used for the charge deformation parameters β_2^c those which reproduce the quadrupole charge distribution moments deduced from Coulomb excitation measurements.[52] We checked that this choice made for β_2^c did not induce appreciable ambiguities in our analysis. On the other hand, as in (d, d') calculations[53] at 12 MeV incident energy, the Coulomb excitation was required to reproduce both the magnitude and the shape of the measured[12] (p, p') angular distributions. The proton optical potential parameters are gathered in Table VI. The Coulomb correction term Δ_c included in the real potential was calculated following Satchler's prescription.[54] The above assumptions yield satisfactory agreement between our calculations and measurements.[12] In addition, fits to angular distributions can be improved at backward angles by taking a proton spin-orbit (so) potential strength $V_{so}(p)$ smaller than that given in Table III for the neutron so potential strength $V_{so}(n)$. This observed trend [i.e., $V_{so}(p) < V_{so}(n)$] is consistent with an isospin-dependent spin-orbit term in the optical potential.[55] The results obtained for ^{184}W using $V_{so}(p) = 4.5$ MeV are shown in Fig. 8. As a short conclusion, these results confirm the utility of proton and neutron scattering experiments for determining complex isospin-dependent terms[54] in the optical potential.

V. MULTIPOLE MOMENTS, VOLUME INTEGRALS, AND rms RADII

The present analysis provides a reliable parametrization of the deformed potential. In order to remove some ambiguities due to the model employed currently and to perform a comparison with some results obtained from (e, e'), (p, p'), (d, d'), (α, α'), muonic atom measurements, and some fundamental calculations we have determined (i) the multipole moments of our optical potential, (ii) the volume integrals and root mean square (rms) radii of the real and imaginary parts of this potential, and (iii) the rms matter radii estimated from the potential radii.

TABLE VI. Even tungsten isotopes. Proton optical potential parameters. Strengths in MeV; geometry parameters in femtometers. Incident proton energy E in MeV; $9 \lesssim E \lesssim 16$ MeV. See Table III for the spin-orbit potential parameters.

$V = 49.90 + 16.00\left(\frac{N-Z}{A}\right) - 0.25E + \Delta_C$	$W_V = 0.20E - 0.80$	$W_D = 8.83 + 8.00\left(\frac{N-Z}{A}\right) - 0.10(E-9)$
$r_V = 1.26$	$r = 1.26$	$r_D = 1.28$
$a_V = 0.63$	$a = 0.63$	$a_D = 0.47$

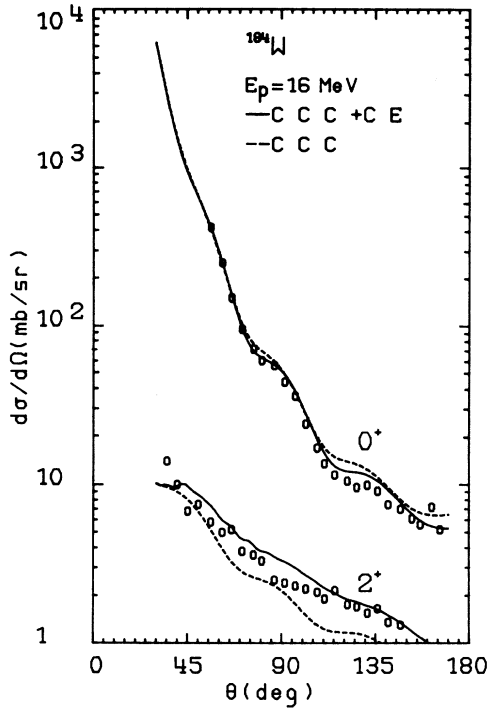

FIG. 8. Proton elastic and inelastic scattering angular distributions at 16 MeV incident energy for ^{184}W. Comparison between measurements (Ref. 12) and coupled-channel calculations (CCC). The full lines are for CCC including Coulomb excitation (CE). The dashed lines are for CCC without Coulomb excitation.

A. Quadrupole and hexadecapole moments $M_{0\lambda}$ (λ = 2,4)

Following Mackintosh[56] one can define normalized potential moments $M^p_{0\lambda}$ for an axially symmetric field as follows:

$$M^p_{0\lambda} = \frac{Z}{J_v} \int V(\vec{r}) r^\lambda Y^0_\lambda(\hat{r})\, d\vec{r}\,, \tag{3}$$

where V is the real part of the optical potential, J_v the volume integral of V:

$$J_v = \int V(\vec{r})\, d\vec{r},$$

and Z is the charge number. The choice made in (3) for $M^p_{0\lambda}$ involves Z rather than A so as to compare the $M^p_{0\lambda}$ values to the charge $M^c_{0\lambda}$ and matter moments $M^m_{0\lambda}$ respectively defined as

$$M^c_{0\lambda} = Z\langle r^\lambda Y^0_\lambda \rangle_z\,, \tag{4}$$

and

$$M^m_{0\lambda} = \frac{Z}{A}\langle r^\lambda Y^0_\lambda \rangle_A\,. \tag{5}$$

In the relations (4) and (5), the brackets $\langle\ \rangle_z$ and

TABLE VII. Tungsten isotopes. Quadrupole and hexadecapole potential and matter moments. The signs + (−) beside moments indicate agreement (disagreement) between these values and respective neutron potential moments of the present work.

	^{182}W		^{183}W		^{184}W		^{186}W	
	M_{02} (e b)	M_{04} (e b^2)	M_{02} (e b)	M_{04} (e b^2)	M_{02} (e b)	M_{04} (e b^2)	M_{02} (e b)	M_{04} (e b^2)
Exp	2.053 [a] (+)	−0.300 [a] (−)			1.940 [a] (−)	−0.243 [a] (+)	1.830 [a] (−)	−0.266 [a] (+)
							1.310 [b] (−)	−0.362 [b] (−)
	2.402 [c] (+)	−0.444 [c] (−)						
					2.394 [d] (−)	0.232 [d] (−)		
	2.166 [e] (+)	−0.195 [e] (+)						
This work	2.222 ± 0.111 [f]	−0.188 ± 0.028 [f]	2.164 ± 0.151 [f]	−0.348 ± 0.070 [f]	2.084 ± 0.063 [f]	−0.227 ± 0.023 [f]	2.033 ± 0.061 [f]	−0.245 ± 0.025 [f]
HFB theory	2.080 [g]	−0.084 [g]			2.032 [g]	−0.160 [g]	1.845 [g]	−0.203 [g]

[a] Potential moments: see Ref. 64.
[b] Potential moments: see Ref. 63.
[c] Potential moments: see Ref. 65.
[d] Potential moments: see Ref. 12.
[e] Potential moments: see Ref. 53.
[f] Present work.
[g] Matter moments: see Ref. 10.

$\langle\,\rangle_A$ represent averaged values of $r^\lambda Y_\lambda^0$ over the charge and matter distributions, respectively. The data reported in the present work are taken from Coulomb excitation measurements[52,57-63] in the Coulomb and Coulomb-nuclear interference region for the charge moments, from inelastic scattering measurements,[12,53,63-65] and compared with Hartree-Fock[66] (HF) and Hartree-Fock-Bogolyubov (HFB) predictions[10] for the charge and matter moments.

The experimental values of the moments are gathered in Tables VII and VIII and compared with the neutron potential moments of the present work and HF and HFB calculations. Some moments, not reported by the quoted authors, were determined. In addition, the (d, d') measurements by Siemssen *et al.*[53] in the Coulomb-nuclear interference region were reanalyzed[67] in the frame of coupled-channel formalism (taking into account the Coulomb excitation) so as to make consistent the comparison between moments.

1. Neutron and charged particle nuclear potential moments

The neutron quadrupole potential moment (NQPM) M_{02}^p of the even isotopes and the odd one is a smoothly decreasing function of the mass number A, while the magnitude of the hexadecapole moments (NHPM) M_{04}^p for the even isotopes increases with A. These trends reflect corresponding variations of the deformation parameters (β_2, β_4) determined in Sec. IV. The NQPM and NHPM values are given in Table VII with their respective uncertainties. These were estimated on the basis of corresponding (β_2, β_4) uncertainties in order to perform a relevant comparison between NQPM and NHPM and other available nuclear potential moments (see Table VII). In the following, we consider two measurements as compatible if they deviate from each other by an amount smaller than twice the standard deviation. Results of this comparison between NQPM and NHPM on the one hand and the other respective moments on the other hand are shown in Table VII. Agreement (disagreement) is noted + (−) beside the compared experimental value. As for the deuteron potential moments for ^{182}W, the good agreement which was obtained is perhaps fortuitous. If one excludes these results, no systematic trend was obtained either for quadrupole or for hexadecapole moments determined in the Coulomb-nuclear interference region. This disappointing conclusion might be related to a previous study by David *et al.*[68] who show a strong interdependence between the potential deformation and the Coulomb deformation when deformations are extracted from (α, α') measurements in the Coulomb-nuclear interference region. The unique agreement between NQPM and alpha-potential moments is provided for (α, α') measurements[65] on ^{182}W well above the Coulomb barrier. Thus, as long as new measurements are not performed, it will be hard to conclude if the disagreement between neutron and charged particle potential moments for W isotopes is real.

TABLE VIII. Tungsten isotopes. Quadrupole and hexadecapole charge moments.

	^{182}W		^{183}W		^{184}W		^{186}W	
	M_{02} (e b)	M_{04} (e b^2)	M_{02} (e b)	M_{04} (e b^2)	M_{02} (e b)	M_{04} (e b^2)	M_{02} (e b)	M_{04} (e b^2)
Exp	2.00 ± 0.05 [a]				1.90 ± 0.05 [a]		1.89 ± 0.07 [a]	
	2.07 ± 0.02 [b]				1.96 ± 0.02 [b]		1.87 ± 0.02 [b]	
	2.04 ± 0.05 [c]				1.91 ± 0.04 [c]		1.88 ± 0.05 [c]	
	2.02 ± 0.01 [d]		1.97 ± 0.03 [d]		1.92 ± 0.01 [d]		1.86 ± 0.02 [d]	
	2.13 [e]							
	2.07 ± 0.025 [f]				1.98 ± 0.025 [f]		1.86 ± 0.025 [f]	
	2.053 ± 0.015 [g]	$-0.63^{+0.34}_{-0.16}$ [g]						
							1.764 ± 0.035 [h]	
							1.636 ± 0.022 [i]	-0.639 ± 0.162 [i]
	2.053 ± 0.015 [j]	$-0.63^{+0.34}_{-0.16}$ [j]			1.94 ± 0.02 [j]	-0.68 ± 0.25 [j]	1.83 ± 0.02 [j]	-0.25 ± 0.25 [j]
$\langle\,\rangle_{exp}$	2.04 ± 0.024 [k]		1.97 ± 0.03 [k]		1.94 ± 0.024 [k]		1.85 ± 0.024 [k]	
Theory	2.053 [l]	−0.076 [l]			2.009 [l]	−0.145 [l]	1.832 [l]	−0.185 [l]
					1.952 [m]	−0.214 [m]		

[a] See Ref. 57.
[b] See Ref. 52.
[c] See Ref. 58.
[d] See Ref. 46.
[e] See Ref. 59.
[f] See Ref. 60.
[g] See Ref. 61.
[h] See Ref. 62.
[i] See Ref. 63.
[j] See Ref. 64.
[k] Averaged values.
[l] See Ref. 10.
[m] See Ref. 66.

2. Neutron potential and charge distribution moments

Many accurate Coulomb-excitation measurements have been performed, at least for the quadrupole moments M^c_{02}. These results and their average values are shown in Table VIII and can be compared to the moments NQPM and NHPM (see Table VII). Both M^c_{02} and M^p_{02} (neutron) behave approximately like linear functions of A, and M^p_{02} exceeds M^c_{02} by about 8%. These trends are not too significant since they are within the uncertainties on M^c_{02} and M^p_{02} (neutron). However, this comparison provides a tendency for M^p_{02} (neutron) to be slightly higher than M^c_{02}.

B. Volume integrals and rms radii

We have also calculated the volume integrals per nucleon (J_v/A and J_w/A) and rms radii ($\langle r_v^2\rangle^{1/2}$ and $\langle r_w^2\rangle^{1/2}$) of the real and imaginary parts of the neutron optical potential. These parameters are defined as follows:

$$J_v/A = A^{-1}\int V(\vec{r})\,d\vec{r},$$

$$J_w/A = A^{-1}\int W(\vec{r})\,d\vec{r},$$

$$\langle r_v^2\rangle^{1/2} = \left[\int r^2 V(\vec{r})\,d\vec{r} \Big/ \int V(\vec{r})\,d\vec{r}\right]^{1/2},$$

$$\langle r_w^2\rangle^{1/2} = \left[\int r^2 W(\vec{r})\,d\vec{r} \Big/ \int W(\vec{r})\,d\vec{r}\right]^{1/2}.$$

The volume integrals J_v/A and J_w/A are given below and rms radii in Table IX. Both these results are given with estimated uncertainties:

$$J_v/A = 455(\pm 10) - 146(\pm 15)[(N-Z)/A] - 2.3(\pm 0.2)E_n \ \text{(MeV fm}^3\text{)}, \quad (6)$$

$$J_w/A = 34(\pm 4) - 55(\pm 14)[(N-Z)/A] + 9(\pm 1)E_n^{1/2} \ \text{(MeV fm}^3\text{)}. \quad (7)$$

The range of validity for relation (6) extends up to $E_n \simeq 15$ MeV. This restriction corresponds to the high energy limit at which a comparison between measured and calculated total cross sections has been done. The volume integral per nucleon J_w/A [Eq. (7)], was determined at incident energies below 9 MeV, where the absorption potential is only of the surface type (see Table III). We have then compared the values of J_v/A [Eq. (6)] determined at $E_n = 5$ MeV with the JLM model[13] predictions reported at this incident neutron energy[69]:

$$J_v/A = 437(\pm 9) - 142(\pm 32)[(N-Z)/A] \ \text{(MeV fm}^3\text{)},$$

and with the systematics established by Kailas and Gupta[69]:

$$J_v/A = \left[440(\pm 9) - 157(\pm 13)\left(\frac{N-Z}{A}\right)\right] \times [1 + 0.06(\pm 0.08)A^{-1/3}].$$

From this comparison it follows that excellent agreement between the values derived from the present work and calculations[13,69] is obtained for the strengths associated with the scalar and isoscalar components of J_v/A. The values of J_v/A, J_w/A, $\langle r_v^2\rangle^{1/2}$, and $\langle r_w^2\rangle^{1/2}$, determined at $E_n = 8$ MeV, are shown in Table IX. These were recently compared (with exception of $\langle r_w^2\rangle^{1/2}$) to the JLM model predictions[14] at this incident energy.[70] Within the uncertainty intervals, the agreement is reasonably good. As for $\langle r_w^2\rangle^{1/2}$, at the same incident neutron energy, the comparison with the JLM model might be questionable since the rms radius $\langle r_w^2\rangle^{1/2}$ is calculated[13] from an absorptive potential W which is not, in general, peaked at the nuclear surface as it is in the present work below 9 MeV.

C. Multipole moments and rms radii of matter distributions

In this subsection the question arises: How can we extract relevant information about the structure of the even W isotopes from our phenomenological optical model analysis? The answer to this question is not obvious since there is no simple relation between optical potential and matter distribution shapes. However, an approach to that subject is provided by the folding model. Following the pioneering work of Greenlees *et al.*,[71] it is common in that model to construct the real part V of the phenomenological optical model potential by folding a local effective interaction t with the nuclear matter density ρ:

$$V(r) = \int t(|\vec{r} - \vec{r}'|)\rho(r')\,d\vec{r}'.$$

In subsequent works, this model was improved by Greenlees, Makofske, and Pyle,[72] who took into account explicitly the isospin term, and by Slanina

TABLE IX. Even tungsten isotopes. $E_n = 8$ MeV. Volume integral (MeV fm^3) and rms radii (fm) for real and imaginary parts of neutron potential. Estimated uncertainties.

Parameter	^{182}W	^{184}W	^{186}W
J_v/A	409 ± 15	408 ± 15	407 ± 15
$\langle r_v^2\rangle^{1/2}$	6.08 ± 0.06	6.09 ± 0.06	6.10 ± 0.06
J_w/A	49 ± 10.0	48.7 ± 10.0	48.5 ± 10.0
$\langle r_w^2\rangle^{1/2}$	7.57 ± 0.30	7.59 ± 0.30	7.61 ± 0.30

and McManus,[73] who generated the real part of the optical potential by folding in more realistic forces rather than using phenomenological interactions. In more recent work, Thomas *et al.*[74] developed a folding model in which the real part of the potential is the sum of direct and exchange terms. It is difficult to appreciate the meaningfulness of the folding model since the interaction t contains adjustable parameters. In addition, t should be nonlocal and energy dependent,[75] and should also contain a dependence on the density of matter similar to that of effective forces used in self-consistent nuclear structure[76] calculations. The relations connecting the potential and the matter moments as well as the rms potential and matter radii are different, depending on whether a density-dependent folding force t was used or not.

Let us first consider the effective interaction t which does not depend on density. In this case we know from a theorem due to Satchler[77] that a folding potential with such an effective force has the same multipole moments $M^p_{0\lambda}$ [Eq. (3)] as those of the nuclear matter density $M^m_{0\lambda}$ [Eq. (5)]. In addition to that property, there exists[71] a simple relation between the folding potential rms radius $\langle r_v^2\rangle^{1/2}$ and the rms point matter density radius $\langle r_m^2\rangle^{1/2}$:

$$\langle r_v^2\rangle = \langle r_m^2\rangle + \langle r_d^2\rangle \,, \tag{8}$$

where $\langle r_d^2\rangle^{1/2}$ is the rms radius of the spin-independent part of the nucleon-nucleon effective force t.

On the contrary, if the effective force t is density dependent (DD) the above properties for multipole moments and rms radii are no longer valid. Examining the extent to which Stachler's theorem breaks down with the use of Green's DD interaction[78] in folding calculations, Hamilton and Mackintosh[79] have shown that

$$M^p_{0\lambda} > M^m_{0\lambda} \quad (\lambda = 2, 4, 6) \tag{9}$$

for some deformed nuclei extending over a large mass range. As for the rms radii, the relation between $\langle r_v^2\rangle^{1/2}$ and $\langle r_m^2\rangle^{1/2}$ should be similar to that given in Eq. (8), provided correction terms to $\langle r_d^2\rangle^{1/2}$ are included. In that respect and following Thomas *et al.*[74] it seems reasonable to define an effective rms radius as follows:

$$\langle r_d^2\rangle_{eff} = \langle r_v^2\rangle - \langle r_m^2\rangle \,, \tag{10}$$

where it is clear that $\langle r_v^2\rangle^{1/2}$ is the rms radius of a folding potential derived from a DD effective interaction. The $\langle r_d^2\rangle_{eff}^{1/2}$ values obtained in Ref. 74 depend on the choice made for the DD effective interactions[78,80,81] and exchange terms. Taking the ^{208}Pb folding potential as an example, one can estimate $\langle r_d^2\rangle_{eff}^{1/2}$ from the folding calculations involving the so-called (WDDE), (SDDE), and (N) density-dependent effective forces considered by Thomas *et al.*[74] We thus obtained the estimated average value

$$\langle r_d^2\rangle_{eff} \simeq 7.0 \text{ fm}^2 \,. \tag{11}$$

In the following discussions we have interpreted the phenomenological optical potential of the present work in the framework of the folding model as outlined above. We have found that (i) the potential and HFB matter moments ($M^p_{0\lambda}$ and $M^m_{0\lambda}$, respectively) gathered in Table VII are in agreement with the previously reported results,[79] Eq. (9), and (ii) the values of rms matter radii deduced from (10) and (11) agree with the corresponding HFB calculations[10] if a density-dependent folding force is considered. For this reason the results obtained in the case of the density-independent folding interaction are not shown.

1. Multipole moments

The comparison between the neutron optical potential moments $M^p_{0\lambda}$ (neutron) and the matter moments $M^m_{0\lambda}$ (HFB) is given in Table VII for $\lambda = 2$ and 4. Although the experimental values are not yet available for the matter moments, the HFB calculations[10] probably give a reliable representation of these moments since the calculated[10] and measured quadrupole charge moments shown in Table VIII are in excellent agreement. The static HFB calculations of Girod and Gogny[10] involve the D1 density-dependent force.[76] These calculations predict values of matter moments smaller than potential moments, as noted above. However, it is worth pointing out that dynamical effects associated with the vibrations could improve such a comparison. In fact, due to the dynamics, we may expect a few percent increase of the matter moments.[82] In spite of that, the relation (9) between potential and matter moments remains unchanged.

2. rms matter radii

In this subsection we present the rms matter radii $\langle r_m^2\rangle^{1/2}$ which have been estimated from the rms radii $\langle r_v^2\rangle^{1/2}$ (Table IX) of our phenomenological optical potential and from $\langle r_d^2\rangle_{eff}$ as given in Eq. (11). We think that the estimation $\langle r_d^2\rangle_{eff} \simeq 7.0$ fm^2 is reliable for the W isotopes since (i) the rms radius of the effective DD folding forces vary slowly[74] with the A-mass number for large values of A, and (ii) this rms radius is nearly energy independent[74] in the energy range considered at present. In view of determining the uncer-

TABLE X. Charge and matter rms radii (fm) for the even tungsten isotopes.

Nuclide		^{182}W	^{184}W	^{186}W
Charge	Exp	5.367 [a]		
		5.449 [b]		
		5.359 [c]	5.370 [c]	5.377 [c]
		5.457 [d]	5.458 [d]	5.432 [d]
			5.425 [e]	5.433 [e]
			5.42 ± 0.07 [f]	5.40 ± 0.04 [f]
	$\langle\ \rangle_{exp}$	5.408 ± 0.054 [g]	5.418 ± 0.054 [g]	5.411 ± 0.054 [g]
	Theory	5.358 [h]	5.370 [h]	5.371 [h]
Matter	This work	5.47 ± 0.12 [i]	5.48 ± 0.12 [i]	5.49 ± 0.12 [i]
	Theory	5.345 [j]	5.362 [j]	5.370 [j]

[a] Charge rms radii: see Ref. 59.
[b] Charge rms radii: see Ref. 61.
[c] Charge rms radii: see Ref. 60.
[d] Charge rms radii: see Ref. 64.
[e] Charge rms radii: see Ref. 83.
[f] Charge rms radii: see Ref. 84.
[g] Averaged values.
[h] Charge rms radii: see Ref. 10.
[i] Matter rms radii: this work.
[j] Matter rms radii: see Ref. 10.

tainty associated with the deduced $\langle r_m^2\rangle^{1/2}$ we have estimated the uncertainty of $\langle r_d^2\rangle_{eff}$. Finally, the adopted value for $\langle r_d^2\rangle_{eff}$ is

$$\langle r_d^2\rangle_{eff} \simeq 7.0 \pm 1.0 \text{ fm}^2 .$$

The point matter radii $\langle r_m^2\rangle^{1/2}$ of the present work are given in Table X where they are compared with HFB calculations.[10] Also shown are the calculated[10] and measured[59-61,64,83,84] rms charge radii $\langle r_c^2\rangle^{1/2}$. The calculations of $\langle r_c^2\rangle^{1/2}$ include center-of-mass correction[80] and proton charge smearing[85] in order to make a meaningful comparison with the respective experimental values. The good agreement between calculations and measurements obtained for $\langle r_c^2\rangle^{1/2}$ make reliable our comparison between the "experimental" (this work) and calculated[10] values of the rms matter radii. Though slightly high, our estimate of $\langle r_m^2\rangle^{1/2}$ agrees with the HFB calculations.[10]

From the estimated $\langle r_m^2\rangle^{1/2}$ values (Table X) it is easy to determine the respective rms neutron radii $\langle r_n^2\rangle^{1/2}$. In doing that, we did not attempt to make an accurate evaluation of $\langle r_n^2\rangle^{1/2}$, which is illusive on the basis of the optical potential now assumed in this paper. Our aim was (i) the estimation of uncertainties on $\langle r_n^2\rangle^{1/2}$ when the optical potential is rather well determined as it is for the tungsten isotopes, and (ii) the comparison between the obtained $\langle r_n^2\rangle^{1/2}$ values and HFB calculations.[10] Starting from the general relation

$$A\langle r_m^2\rangle = N\langle r_n^2\rangle + Z\langle r_p^2\rangle ,$$

where $\langle r_p^2\rangle^{1/2}$ is the rms proton radius and $N(Z)$ the neutron (proton) number, we determined $\langle r_n^2\rangle^{1/2}$. The $\langle r_p^2\rangle^{1/2}$ values are obtained from $\langle r_c^2\rangle^{1/2}$ (exp) (see Table X) by removing proton charge smearing. We thus obtained $\langle r_n^2\rangle^{1/2}$ values slightly higher than $\langle r_p^2\rangle^{1/2}$ values. These results may be summarized as follows:

$$\langle r_n^2\rangle^{1/2}/\langle r_p^2\rangle^{1/2} = 1.04 \pm 0.04 ,$$

where most of uncertainties come from the rms radius of the two-body folding force. The HFB calculations[10] lead to

$$\langle r_n^2\rangle^{1/2}/\langle r_p^2\rangle^{1/2} = 1.02 .$$

Once again, our results are in agreement with the Hartree-Fock-Bogolyubov calculations.[10] In the present work the uncertainty in the neutron rms radii $\langle r_n^2\rangle^{1/2}$ is found to be ±0.21 fm. This value is large when compared to the typical error (±0.07 fm) on the same quantity determined[86] from an analysis of 800 MeV polarized proton scattering from some nuclei.

VI. CONCLUSION

The aim of the present work was the investigation of shapes and deformations by using fast neutron scattering on tungsten isotope samples. For that purpose, elastic and inelastic scattering angular distributions were accurately measured at an energy of 3.4 MeV and analyzed in terms of a deformed optical potential assuming the axially symmetric rotational model for the even (^{182,184,186}W) as well as the odd (^{183}W) isotopes. Though the simultaneous analysis of total cross sections σ_T available at the beginning of our work was difficult, the coherence of our calculation methods led to a satisfactory agreement with most of the recent neutron cross section measurements. Finally, the above optical potential is suitable for the description of cross sections in the energy

interval 300 keV–15 MeV. Below a few hundred keV incident energy a disagreement remains between the available σ_T data and calculations. One of our preoccupations was the careful determination of hexadecapole deformation parameters β_4. We thus found large and unambiguously negative values for them. These results agree well with nuclear structure studies based on Nilsson type and Hartree-Fock-Bogolyubov calculations. From the simultaneous analysis of neutron and proton cross sections we establish that the nucleon optical potential is isospin dependent in the tungsten mass region. The isoscalar component of this potential is complex and its imaginary part is small. Most of the properties of the deformed optical potential agree with the JLM model. The analysis of our potentials provides multipole moments and rms radii. For the even isotopes the quadrupole moment values decrease with increasing mass number while hexadecapole moment values increase. More interesting are the moments obtained for ^{183}W: the main effect of adding one neutron to the ^{182}W core results in a strong increase of the hexadecapole potential moment. If true, this property should be reproduced in Hartree-Fock-Bogolyubov calculations involving an odd neutron blocked in a quasiparticle orbit. For the even isotopes the comparison between neutron and available deuteron and alpha potential moments provides contradictory results. The only significant agreement between quadrupole moments is obtained for alpha particle scattering from ^{182}W at an incident energy well above the Coulomb barrier. The origin of observed deviations of charged particle potential moments measured in the Coulomb-nuclear interference region from neutron potential moments is not definitely established. This might be related to the ambiguity in the determination of both Coulomb and nuclear potential moments. Then we emphazised the comparison between quadrupole potential (M^p_{02}) and matter (M^m_{02}) moments. The A-mass dependences of these moments are quite similar. Moreover, it appears that M^p_{02} is slightly higher than M^m_{02}. If this result is significant, it should imply the inapplicability of Satchler's theorem. Consequently, if further optical model analysis is performed, it should be done in the framework of a folding model involving a density-dependent effective force. Finally, if a density-dependent folding interaction is assumed, the rms matter radii extracted from our phenomenological potential analysis are in agreement with the Hartree-Fock-Bogolyubov predictions.

ACKNOWLEDGMENTS

The authors wish to express their gratitude to M. Girod and D. Gogny for giving them the HFB calculations prior to publication, and Dr. A. B. Smith for providing the W total cross sections which were recently measured at Argonne National Laboratory. Finally, they thank Dr. J. Raynal and Dr. Ch. Lagrange for useful discussions.

[1]J. Lachkar, G. Haouat, J. Sigaud, Y. Patin, F. Coçu, C. Humeau, and S. Seguin, CEA Report No. CEA-R-4839 (1977).

[2]J. Lachkar, in *Proceedings of an International Conference on Neutron Physics and Nuclear Data for Reactors and Other Applied Purposes, Harwell, U. K., 1978* (OCDE/Nuclear Energy Agency, Paris, 1978), p. 136.

[3]W. Glasgow and D. Graham Foster, Phys. Rev. C 3, 604 (1971).

[4]H. Marshak, A. Langsford, C. Y. Wong, and T. Tamura, Phys. Rev. Lett. 20, 554 (1968).

[5]G. Palla, Phys. Lett. 35B, 477 (1971).

[6]Ch. Lagrange, R. E. Shamu, T. Burrows, G. P. Glasgow, G. Hardie, and F. D. McDaniel, Phys. Lett. 58B, 293 (1975); R. E. Shamu, Ch. Lagrange, E. M. Bernstein, J. J. Ramirez, T. Tamura, and C. Y. Wong, *ibid.* 61B, 29 (1976).

[7]M. T. McEllistrem, R. E. Shamu, J. Lachkar, G. Haouat, Ch. Lagrange, Y. Patin, J. Sigaud, and F. Coçu, Phys. Rev. C 15, 927 (1977).

[8]U. Götz, H. C. Pauli, and K. Alder, Nucl. Phys. A192, 1 (1972).

[9]P. Möller, S. G. Nilsson, and J. R. Nix, Nucl. Phys. A229, 292 (1974).

[10]M. Girod and D. Gogny (private communication).

[11]Ch. Lagrange, J. Phys. (Paris) Lett. 35, 111 (1974).

[12]T. Kruse, W. Makofske, H. Ogata, W. Savin, M. Slagowitz, M. Williams, and P. Stoler, Nucl. Phys. A169, 177 (1971).

[13]J. P. Jeukenne, A. Lejeune, and C. Mahaux, ERDA Report No. CONF-76Q715-P1, 1976; Phys. Rep. 25C, 83 (1976); Phys. Rev. C 15, 10 (1977); 16, 80 (1977).

[14]A. Lejeune (private communication to Ch. Lagrange).

[15]J. Lachkar, M. T. McEllistrem, G. Haouat, Y. Patin, J. Sigaud, and F. Coçu, Phys. Rev. C 14, 933 (1976).

[16]H. Liskien and A. Paulsen, At. Data Nucl. Data Tables 15, 57 (1975).

[17]W. E. Kinney, Nucl. Instrum. Methods 83, 15 (1970).

[18]M. Sakai and A. C. Rester, At. Data and Nucl. Data Tables 20, 441 (1977); A. Artna-Cohen, Nucl. Data Sheets 16, 267 (1975).

[19]K. Kumar and M. Baranger, Nucl. Phys. A122, 273 (1968).

[20]A. K. Kerman, K. Dan. Vidensk. Selsk. Mat. Fys. Medd. 30, No. 15 (1956).

[21]D. J. Rowe, Nucl. Phys. 61, 1 (1965).

[22]R. T. Brockmeier, S. Wahlborn, E. J. Seppi, and

F. Boehm, Nucl. Phys. 63, 102 (1965).
[23]J. P. Delaroche, Ch. Lagrange, and J. Salvy, in *Nuclear Theory in Neutron Nuclear Data Evaluation* (IAEA, Vienna, 1976), Vol. II, p. 251.
[24]S. F. Mughabghab and D. I. Garber, BNL Report No. BNL-325 (1973), 3rd ed., Vol. 1.
[25]Z. M. Bartolome, R. W. Hockenbury, W. R. Moyer, J. R. Tatarczuk, and R. C. Block, Nucl. Sci. Eng. 37, 137 (1969).
[26]H. S. Camarda, H. I. Liou, G. Hacken, F. Rahn, W. Makofske, M. Slagowitz, S. Wynchank, and J. Rainwater, Phys. Rev. C 8, 1813 (1973).
[27]A. A. Bergman, S. P. Kapchigashev, Yu. P. Popov, and S. A. Romanov, in *Proceedings of the International Conference on the Study of Nuclear Structure with Neutrons, Antwerp, 1965* (North-Holland, Amsterdam, 1966), p. 570.
[28]J. Whalen and J. Meadows, ANL Report No. ANL-7210 (1966).
[29]R. C. Martin, Bull. Am. Phys. Soc. 12, 106 (1967); Ph.D. thesis, Rensselaer Polytechnic Institute, 1967 (unpublished).
[30]F. D. Becchetti, Jr. and G. W. Greenlees, Phys. Rev. 182, 1190 (1969).
[31]H. Sherif and J. S. Blair, Phys. Lett. 26B, 489 (1968).
[32]J. Raynal, ECIS 78 (unpublished).
[33]J. Raynal, in *Proceedings of the Symposium on Nuclear Reaction Mechanisms and Polarization Phenomena, 1969* (Les Presses de l'Université Laval, Québec, 1970), p. 75.
[34]Ch. Lagrange and N. Mondon, internal report, Centre d'Etudes de Limeil, France, 1973 (unpublished).
[35]T. Tamura, ORNL Report No. ORNL-4152, 1967.
[36]Ch. Lagrange and B. Duchemin, HELMAG (unpublished).
[37]P. A. Moldauer, Phys. Rev. C 11, 426 (1975); 14, 764 (1976). J. W. Tepel, H. M. Hofmann, and H. A. Weidenmüller, Phys. Lett. 49B, 1 (1974). H. M. Hofmann, J. Richert, J. W. Tepel, and H. A. Weidenmüller, Ann. Phys. (N.Y.) 90, 403 (1975).
[38]P. A. Moldauer, Phys. Rev. C 12, 744 (1975).
[39]Ch. Lagrange, in *Proceedings of a Specialist's Meeting Held at the Central Bureau of Nuclear Measurements, Geel, Belgium, 1977*, edited by K. H. Böckhoff (Pergamon, N. Y., 1979).
[40]L. Dresner, ORNL Report No. ORNL-CF-57-6-2, 1957.
[41]C. M. Perey and F. G. Perey, At. Data Nucl. Data Tables 17, 10 (1976).
[42]D. Lister, A. Smith, and C. Dunford, Phys. Rev. 162, 1077 (1967).
[43]A. R. de L. Musgrove, AAEC Report No. AAEC/E277, 1973.
[44]J. P. Delaroche (unpublished).
[45]A. B. Smith (private communication).
[46]K. E. G. Löbner, M. Vetter, and V. Hönig, Nucl. Data Tables 7, 495 (1970).
[47]R. F. Casten, D. Breitig, O. A. Wasson, K. Rimawi, and R. E. Chrien, Nucl. Phys. A228, 493 (1974).
[48]R. F. Casten, Phys. Lett. 49B, 258 (1974).
[49]F. M. Bernthal, B. D. Jeltema, J. S. Boyno, T. L. Khoo, and R. A. Warner, Phys. Rev. Lett. 33, 915 (1974).
[50]G. E. Brown, *Unified Theory of Nuclear Models and Forces* (North-Holland, Amsterdam, 1967), p. 163.
[51]The full consistent determination of the isospin potential requires, in addition, to fit on (p,n) cross sections leading to isobaric analog states. Unfortunately such measurements are not available for the tungsten isotopes.
[52]R. G. Stokstad and B. Persson, Phys. Rev. 170, 1072 (1968).
[53]R. H. Siemssen and J. R. Erskine, Phys. Rev. 146, 911 (1966).
[54]G. R. Satchler, *Isospin Dependence of Optical Model Potentials in Isospin in Nuclear Physics*, edited by D. H. Wilkinson (North-Holland, Amsterdam, 1969), p. 389.
[55]J. Gosset, B. Mayer, and J. L. Escudié, Phys. Rev. C 14, 878 (1976).
[56]R. S. Mackintosh, Nucl. Phys. A266, 379 (1976).
[57]O. Hansen, M. C. Olesen, O. Skilbreid, and B. Elbek, Nucl. Phys. 25, 634 (1963).
[58]P. H. Stelson and L. Grodzins, Nucl. Data Sec. A1, 21 (1965).
[59]J. P. Davidson, D. A. Close, and J. J. Malanify, Phys. Rev. Lett. 32, 337 (1974).
[60]D. Hitlin, S. Bernow, S. Devons, I. Duerdoth, J. W. Kast, E. R. Macagno, J. Rainwater, C. S. Wu, and R. C. Barrett, Phys. Rev. C 1, 1184 (1970).
[61]C. E. Bemis, Jr., P. H. Stelson, F. K. McGowan, W. T. Milner, J. L. C. Ford, Jr., R. L. Robinson, and W. Tuttle, Phys. Rev. C 8, 1934 (1973).
[62]W. T. Milner, F. K. McGowan, R. L. Robinson, P. H. Stelson, and R. O. Sayer, Nucl. Phys. A177, 1 (1971).
[63]W. Brückner, D. Husar, D. Pelte, K. Traxel, M. Samuel, and U. Smilansky, Nucl. Phys. A231, 159 (1974).
[64]I. Y. Lee, J. X. Saladin, J. Holden, J. O'Brien, C. Baktash, C. Bemis, Jr., P. H. Stelson, F. K. McGowan, W. T. Milner, J. L. C. Ford, Jr., R. L. Robinson, and W. Tuttle, Phys. Rev. C 12, 1483 (1975).
[65]D. L. Hendrie, B. G. Harvey, J. C. Faivre, and J. Mahoney, UCRL Report No. UCRL-20426, 1970, p. 87.
[66]H. Flocard, Ph. Quentin, and D. Vautherin, Phys. Lett. 46B, 304 (1973).
[67]J. P. Delaroche; the results of this deformed potential analysis, not shown in the present paper, are available on request.
[68]P. David, J. Debrus, H. Essen, F. Lübke, H. Mommsen, R. Schoenmackers, W. Soyez, H. V. Geramb, and E. F. Hefter, Z. Phys. A 278, 281 (1976).
[69]S. Kailas, and S. K. Gupta, Phys. Rev. C 17, 2236 (1978).
[70]Ch. Lagrange and J. P. Delaroche, in *Proceedings of an International Conference on Neutron Physics and Nuclear Data for Reactors and Other Applied Purposes, Harwell, U. K., 1978* (OCDE/Nuclear Energy Agency, Paris, 1978), p. 355.
[71]G. W. Greenlees, G. J. Pyle, and Y. C. Tang, Phys. Rev. 171, 1115 (1968).
[72]G. W. Greenlees, W. Makofske, and G. J. Pyle, Phys. Rev. C 1, 1145 (1970).
[73]D. Slanina and H. McManus, Nucl. Phys. A116, 271 (1968).
[74]G. L. Thomas, B. C. Sinha, and F. Duggan, Nucl. Phys. A203, 305 (1973).
[75]J. P. Jeukenne, A. Lejeune, and C. Mahaux, in *Proceedings of the International Conference on Nuclear*

Self-Consistent Fields, Trieste, 1975, edited by G. Ripka and M. Porneuf (North-Holland, Amsterdam, 1975), p. 155.
[76]D. Gogny, in *Proceedings of the International Conference on Nuclear Self-Consistent Fields, Trieste, 1975,* edited by G. Ripka and M. Porneuf (North-Holland, Amsterdam, 1975), p. 333.
[77]G. R. Satchler, J. Math. Phys. 13, 1118 (1972).
[78]A. M. Green, Phys. Lett. 24B, 384 (1967).
[79]J. K. Hamilton and R. S. Mackintosh, J. Phys. G 3, L19 (1977).
[80]J. W. Negele, Phys. Rev. C 1, 1260 (1970).
[81]V. R. Pandharipande, Nucl. Phys. A135, 419 (1969).
[82]K. Kumar (private communication).
[83]I. Y. Lee, J. X. Saladin, C. Baktash, J. E. Holden, and J. O'Brien, Phys. Rev. Lett. 33, 383 (1974).
[84]D. Kalinsky, L. S. Gardman, R. Yen, J. R. Legg, and C. K. Bockelman, Nucl. Phys. A216, 312 (1973).
[85]F. Borkowski, G. G. Simon, V. H. Walther, and R. D. Wendling, Z. Phys. A 275, 29 (1975).
[86]L. Ray, W. Rory Coker, and G. W. Hoffmann, Phys. Rev. C 18, 2641 (1978).